Temporal scaling phenomena in groundwater-floodplain systems using robust detrended fluctuation analysis

Abrar Habib[1], James P.R . Sorensen[2], John P. Bloomfield[2], Katie Muchan[3], Andrew J. Newell[2], Adrian P. Butler[1].

[1] Department of Civil and Environmental Engineering, Imperial College London, London, SW7 2AZ, UK

[2] British Geological Survey, Maclean Building, Crowmarsh Gifford, Wallingford, Oxon, OX10 8BB, UK

[3]Centre for Ecology and Hydrology, Maclean Building, Crowmarsh Gifford, Wallingford, Oxon, OX10 8BB, UK

Correspondence author: Abrar Habib, abrar.habib11@imperial.ac.uk or abr.habib@gmail.com

Abstract

In order to determine objectively the fractal behaviour of a time series, and to facilitate potential future attempts to assess model performance by incorporating fractal behaviour, a multi-order robust detrended fluctuation analysis (r-DFAn) procedure is developed herein. The r-DFAn procedure allows for robust and automated quantification of mono-fractal behaviour. The fractal behaviour is quantified with three parts: a global scaling exponent, crossovers, and local scaling exponents. The robustness of the r-DFAn procedure is established by the systematic use of robust regression, piecewise linear regression, Analysis of Covariance (ANCOVA) and Multiple Comparison Procedure to determine statistically significant scaling exponents and optimum crossover locations. The MATLAB code implementing the r-DFAn procedure has also been open sourced to enable reproducible results.

r-DFAn will be illustrated on a synthetic signal after which is used to analyse high-resolution hydrologic data; although the r-DFAn procedure is not limited to hydrological or geophysical time series. The hydrological data are 4 year-long datasets (January 2012 to January 2016) of 1-minute

groundwater level, river stage, groundwater and river temperature, and 15-minute precipitation and air temperature, at Wallingford, UK. The datasets are analysed in both time and fractal domains. The study area is a shallow riparian aquifer in hydraulic connection to River Thames, which traverses the site. The unusually high resolution datasets, along with the responsive nature of the aquifer, enable detailed examination of the various data and their interconnections in both time- and fractal-domains.

Keywords: robust detrended fluctuation analysis; detrended fluctuation analysis; fractal behaviour; Hurst Phenomenon; Time series analysis; high resolution hydrological data;

Introduction

In the field of hydrology, the onset of the study of fractal behaviour of hydrological time series is marked with Hurst's investigation of the storage capacity of the Aswan High Dam in Egypt in 1951 (Hurst 1956, Hurst 1951). This sparked further investigation of what later came to be known as the 'Hurst Phenomenon' (Hurst 1951). The initial mathematical representation of the Hurst Phenomenon was described in terms of range, standard deviation and the number of samples considered. However, this relationship evolved into: $E\{X(T)\} \propto T^H \text{ with } H \neq 0.5$, where $X(T)$ is the aggregated series at scale T and H is the Hurst Exponent (Bras, Rodriguez-Iturbe 1985). Of course, the relationship follows a power law and is linearly related to other measures of fractal behaviour such as the power-law exponent of the spectral density estimate and the scaling exponent α determined by detrended fluctuation analysis.

The mathematician Benoit Mandelbrot introduced a different concept to the Hurst Phenomenon that infuses the self-similarity property of fractals with that of Hurst (Mandelbrot 1982). Mandelbrot introduced the term 'fractional noises' in 1968 to unify the different terms developed over time and across the different fields that describe series with long-term interdependence (Mandelbrot, Van Ness

1968). Hence the term 'Fractal behaviour' will be used in this paper to refer to the 'Hurst phenomenon' and 'long-term memory'; terms which are more common to hydrologists.

Evidently, fractal behaviour of time series has been investigated in various fields and a wide variety of techniques have been used to quantify it. Fractal behaviour has been studied in the fields of, amongst others, pharmacology: long-term correlations of DNA (Peng, Buldyrev et al. 1994); cardiology: non-stationary heart beat time series (Peng, Havlin et al. 1995); earth sciences: ocean wave height (Ozger 2011), temperature (Koscielny-Bunde, Bunde et al. 1996) and seismicity (Alvarez-Ramirez, Echeverria et al. 2011); traffic control: traffic speeds time series (Shang, Lu et al. 2008), in marine transportation (Chen, Tian et al. 2016), solar physics: sunspot time series (Sadegh Movahed, Jafari et al. 2006), finance: the economy and stock market (Reboredo, Rivera-Castro et al. 2013) (Zunino, Tabak et al. 2008, Caraiani 2012) and even in music (Dagdug, Alvarez-Ramirez et al. 2007, Jafari, Pedram et al. 2012, Hennig, Fleischmann et al. 2011, Telesca, Lovallo 2012). Finally, it has been widely used to investigate the fractal behaviour of hydrological systems, which is the focus of this investigation.

A variety of techniques have been used to study the fractal behaviour of time series. These include spectral analysis, wavelet analysis, rescaled-range (R\S), and detrended fluctuation analysis (DFA). Among these techniques, DFA and spectral analysis are the most commonly used, with DFA being the preferred technique by many researchers (Chen, Ivanov et al. 2002, Eichner, Koscielny-Bunde et al. 2003, Zhang, Zhou et al. 2011, Hu, Ivanov et al. 2001, Matsoukas, Islam et al. 2000, Hu, Gao et al. 2009, Ozger 2011) due to ease of detecting changes in scaling when compared to spectral analysis. Many hydrological time series are mono- and multi-fractal in nature with cut-offs in their scaling regime, i.e. they exhibit crossovers (Little, Bloomfield 2010, Matsoukas, Islam et al. 2000, Li, Zhang 2007, Tessier, Lovejoy et al. 1996). Identifying these crossovers, or scaling breakpoints, is not generally done in a systematic or objective way, if it is acknowledged at all (Little, Bloomfield 2010, Zhang, Zhou et al. 2011, Zhu, Young et al. 2012, Williams, Pelletier 2015, Yu, Ghasemizadeh et al. 2016, Li, Mu et al. 2015, Condon, Maxwell 2014). In order to overcome this deficiency and to provide a means for quantifying reliable mono-fractal behaviour that can be used for further analysis – such as in conjunction with models or to infer causalities – this study presents a robust DFA procedure, named r-DFAn. The aim behind r-DFAn is to identify statistically different scaling regions in a signal along with the location of these changes, or crossovers, in a systematic way.

Even though fractal behaviour was found to be intrinsic to signals observed from diverse fields, a key stage in its development is Hurst's investigation of the storage capacity of the Aswan High Dam in Egypt in 1951. Analysing annual flows in the Nile, he noticed the clustering of high flows and low flows in the hydrological time series, and how these variations were scaled with the time over which they were considered. This effect came to be known as the Hurst Phenomenon (Hurst 1956, Hurst 1951) and appears to be a fundamental property of many natural and anthropogenic systems, as the above examples show.

Hydrological and hydro-meteorological time series such as rainfall, river stage, river flow, temperature and more recently, groundwater levels have been characterised as being fractal (Eichner, Koscielny-Bunde et al. 2003, Zhang, Schilling 2004, Zhang, Yang 2010, Fraedrich, Larnder 1993, Gelhar 1974, Kavasseri, Nagarajan 2004, Li, Zhang 2007, Little, Bloomfield 2010, Zhu, Young et al. 2012, Liang, Zhang 2013), however, high resolution hydrological datasets are generally not available and this makes the study of the full range of fractal behaviour difficult. Among hydrological variables, groundwater levels, in particular, are not generally monitored at very short time intervals (such as one minute intervals), as for most purposes less frequent measurements are considered sufficient to capture any variations of interest. Indeed, in many aquifers the forcing processes are significantly damped such that there is very little value in monitoring at time intervals less than 1 day. However, this is not necessarily the case for shallow permeable aquifers, particularly if hydraulically connected with a river. In such cases, fluctuations in recharge due to variations in rainfall or changes in river stage during flood events can cause sub-daily groundwater level variations which can only be studied with high resolution data.

After presenting the r-DFAn procedure, a synthesized mono-fractal signal will be used to illustrate r-DFAn. In addition to this, high resolution, 1-minute and 15-minute, hydrological data from a study site in Wallingford will be presented in the time domain and their fractal behaviour will be analysed using r-DFAn. The datasets are: groundwater levels, river stage, groundwater temperature, river temperature, precipitation and air temperature.

The sections that follow include an explanation of the r-DFAn procedure followed by a detailed description of the study site and data collection and finally a presentation of the r-DFAn results along with a general discussion and some conclusions.

Methodology: r-DFAn procedure

Among numerous methods developed for studying fractal behaviour, detrended fluctuation analysis (DFA) is agreed to be a reliable method for non-stationary signals (Chen, Ivanov et al. 2002, Eichner, Koscielny-Bunde et al. 2003, Zhang, Zhou et al. 2011, Hu, Ivanov et al. 2001, Matsoukas, Islam et al. 2000), among others). Nevertheless, in the case of mono-fractal signals that exhibit changes in there scaling regimes, determining crossovers is subjective and seriously affects the reliability of mono-fractal quantification.

Hence a procedure that includes DFA and statistical models was developed in order to overcome this shortcoming and to automate the entire quantification process. The procedure, which will be named r-DFAn, where n is the order of the detrending function, is explained below and illustrated on a synthetic signal.

Detrended fluctuation analysis

DFA of first order (i.e. DFA1) was first proposed by (Peng, Buldyrev et al. 1994) when analysing correlations in DNA. DFA is presented in the following five steps:

1. Let $y(t_i)$ be a measurement of variable y observed at equally spaced time intervals, t_i, for N discrete times. Let $\overline{y}$ be the mean of $y(t_i)$. Compute $Y(t_i)$ by subtracting the mean from the time series and computing a cumulative sum:

$$Y(t_i) = \sum_{i=1}^{N} \left(y(t_i) - \bar{y} \right) \tag{1}$$

2. Divide $Y(t_i)$ into m non-overlapping segments each of length L so that $m = int\left(\frac{N}{L}\right)$. Each segment will be notated as $Y_{j,k}(t_i)$ where $j = 1, 2, \ldots L$ and $k = 1, 2, \ldots m$, hence $i = (k-1)L + j$.
3. Determine the variance ($F_k^2(L)$) of the fluctuation in each segment (Y_k) after subtracting a best-fit polynomial of order n ($P_{j,k}^n(t_i)$) from each segment. DFAn refers to DFA detrending with polynomial of order n.

$$F_k^2(L) = \frac{1}{L} \sum_{j=1}^{L} \left(Y_{j,k} - P_{j,k}^n \right)^2 \quad for\, k = 1, 2, \ldots m \tag{2}$$

4. Determine an average variance measure for all segments of length L :

$$F(L) = \left[\frac{1}{m} \sum_{k=1}^{m} F_k^2(L) \right]^{1/2} \tag{3}$$

5. Repeat steps 1 to 4 for different values of L then plot $F(L)$ versus L on logarithmic axes to determine the scaling exponent (α) which is the slope of a best-fit line, as:

$$F(L) \approx L^{\alpha} \tag{4}$$

In this paper, α will be referred to as the global scaling exponent; the slope determined by ignoring the occurrence of any local changes in the scaling exponent. Robust regression (with a bi-square weight function) is used to determine α. This ensures that the scaling exponent so determined is based on residuals that are within predefined bounds.

Determining scaling exponents and crossovers for mono-fractal signals

As previously mentioned, changes in the slope of the scaling exponent (α) may be observed, which indicate mono-fractal behaviour with changes in the scaling regime. The time periods (L) where such changes occur are referred to as crossovers (Kantelhardt, Koscielny-Bunde et al. 2001, Hu, Ivanov et al. 2001, Li, Zhang 2007). Even though DFA is a reliable method for identifying fractal behaviour, determining the number and locations of crossovers, has been rather subjective.

After determining the global scaling exponent using robust regression, piecewise linear regression will be used to optimise the locations of crossovers by minimising the least squares error between the data and the fitted broken-line (i.e. the line with crossovers). The number of crossovers to be fitted to the data are determined in order to give the maximum number of crossovers that produce significantly different slopes based on a 95% significance level. This is determined by applying an analysis of covariance (ANCOVA) and a multiple comparison procedure on the DFA results. The number of crossovers are progressively increased until the method fails to yield any further significant scaling exponents.

ANCOVA (the analysis of covariance) is a statistical model that combines both ANOVA (analysis of variance) and linear regression. ANOVA tests the hypothesis that the groups of a dependent variable are significantly different from a categorised independent variable, based on a given significance level. When combining linear regression with ANOVA, the slopes of the groups of the dependent variable can be tested to see whether they are collectively significantly different or not. Hence, by using the F-test, ANCOVA tests the hypothesis that all groups are significantly different against the null hypothesis that they are all the same. For comparisons between adjacent slopes, as opposed to an overall test as in ANCOVA, a multiple comparison procedure is performed post-hoc ANCOVA. With comparisons between three or more groups, simultaneous statistical inferences increase the chances of falling into type I error. Multiple comparisons procedure avoids this by increasing the threshold for inferences.

As an aside, least squares regression (which is conventionally used for determining scaling exponents for DFA) and other statistical models adopted herein, are based on the assumption of independence of residuals. However, this is not true when it comes to DFA data points due to the method of their computation which involves an overlap of segments when determining $F(L)$ for the different time scales.

Crossovers and artefacts in DFA results

Crossovers observed when analysing DFA results may either be indicative of a true difference in the scaling behaviour of the fluctuations or may be induced due to non-stationarities or periodicity inherent in the data (Kantelhardt, Koscielny-Bunde et al. 2001, Chen, Ivanov et al. 2002, Hu, Ivanov et al. 2001). (Kantelhardt, Koscielny-Bunde et al. 2001) have studied in detail the effects of a polynomial or oscillatory trend on DFA results and show that higher order DFA can, in many cases, help in determining true correlation of the fluctuations and the cause behind the occurrence of a crossover. This systematic handling of trends and periodicity gives DFA an advantage over other non-detrending methods (Kantelhardt, Koscielny-Bunde et al. 2001).

In previous studies researchers removed periodicity in a time series prior to DFA in order to determine 'true scaling exponents' ((Sadegh Movahed, Jafari et al. 2006, Li, Zhang 2007, Hu, Ivanov et al. 2001, Kavasseri, Nagarajan 2004)). In this study, periodicity is considered to be part of the fluctuation structure that is naturally induced by meteorological and hydrological processes, and hence will not be removed and instead will be identified in the fractal behaviour. In addition, since hydrological datasets are generally quasi-periodic, removal of periodicity inevitably leads to unintended modification or addition of trends or a smoothing of the fluctuations.

The scaling behaviour of a time series is approached asymptotically, hence high order DFA results deviate from a co-linear trend at smaller time scales and this affects the determined scaling exponent (Kantelhardt, Koscielny-Bunde et al. 2001). This deviation is overcome by dividing $F\left(L\right)$ by a correction factor $K\left(s\right)$, which in turn is determined by averaging over configurations of surrogate datasets that are Monte-Carlo simulations of the original time series (100 configurations will be used in this study) to obtain a modified variance measure, $F_{\mathrm{mod}}^{(n)}\left(L\right)$ (Kantelhardt, Koscielny-Bunde et al. 2001):

$$F_{\mathrm{mod}}^{(n)}(L) = \frac{F^{(n)}(L)}{K_{1/2}^{(n)}(L)} = F^{(n)}(L)\frac{\left\langle \left[F_{shuff}^{(n)}(\mathrm{L}')\right]^{2}\right\rangle^{1/2} L^{1/2}}{\left\langle \left[F_{shuff}^{(n)}(L)\right]^{2}\right\rangle^{1/2} \mathrm{L}'^{1/2}} \quad \text{for } \mathrm{L}' \approx \mathrm{N}/20 \qquad (5)$$

Where $\langle ... \rangle$ denotes the average over all configurations and $F^{(n)}(\mathrm{L})$ denotes the computed variance measure from step 4 using nth order DFA, i.e. DFAn.

Figure 1 presents a flowchart, which summarises the r-DFAn procedure explained above.

Illustration of r-DFAn

Here r-DFAn involves performing r-DFA1 to r-DFA6 after which artificial deviations in fractal behaviour are resolved by using equation (5). The global scaling exponent is then determined for all DFA orders using robust regression with bi-square weighting. This is followed by determining crossovers (if any) using piecewise linear regression, the results of which are analysed using ANCOVA, and, in turn, the results from the ANCOVA are assessed using a multiple comparison procedure in order to ensure that the chosen number of crossovers are statistically significant. The code has been made available online in (Habib 2016).

A synthesized mono-fractal signal with specified scaling behaviour and crossover location is used to illustrate the r-DFAn method. The fractal signal is generated using Fourier analysis by scaling white noise in the frequency domain in order to produce a power spectral density that possesses a certain known scaling behaviour (Kantelhardt, Koscielny-Bunde et al. 2001). This is generated as follows:

1. Fourier transform a realisation of white noise from time domain ($u(t)$) to frequency domain ($u(f)$):

$$u(f) = \int_{-\infty}^{\infty} u(t) e^{-2\pi itf} dt \tag{6}$$

2. Scale the obtained power spectral density according to the following equation:

$$F(f) = u(f) \times \left(\frac{f_{CO}}{f} \right)^{\frac{2\alpha - 1}{2}} \tag{7}$$

   Where f_{CO} is the frequency corresponding to crossover t_{CO}, and $\alpha = \begin{cases} \alpha_1 & \text{for } f \le f_{CO} \\ \alpha_2 & \text{for } f > f_{CO} \end{cases}$.

3. Repeat steps (1) and (2) N times and compute the average power spectral density estimate:

$$F_{av}(f) = \langle F(f) \rangle_n \quad (8)$$

Where $\langle ... \rangle_n$ is the average over n configurations.

4. Perform inverse Fourier transform on the computed average power spectral density to obtain a mono-fractal signal in the time domain with a crossover in the scaling regime:

$$F(t) = \int_{-\infty}^{\infty} F_{av}(f) e^{2\pi i f t} df \quad (9)$$

$F(t)$ is obtained using 100 configurations of a series of length 2^{21} = 2,097,152 data points, and with a crossover, in the time domain, at 500 time units and a scaling exponent of 1.0 and 0.5 before and after the crossover respectively (Figure 2). r-DFAn is used to determine statistically significant scaling exponents of the synthesized signal and the results are presented in Figure 3.

r-DFAn produced results similar to that in Kantelhardt, Koscielny-Bunde et al. (2001) where the crossover locations lie ahead of the theoretical location and moves forward on the time scale axis with the increase in DFA order. The persistence of the crossover across all r-DFA orders indicates that there is a change in the scaling regime. The fluctuation structure of the series at all time scales is intertwined. This is evident from the determined scaling exponents where the segment that should possess a SE of exactly 1.0, exhibits a SE less than 1.0 and the segment that should possess a SE of exactly 0.5 tends to exhibit a SE higher than 0.5. This shows how the white noise segment and the rescaled structured noise segment inevitably affect each other, and in-turn, affect the location of the crossover.

The crossovers in Figure 3 are compared by plotting them against the respective DFA order (Figure 4). Evidently, the crossover value progresses across DFA orders following a linear trend.

To the best of our knowledge, the following three publications introduced methods for objective fractal behaviour identification using DFA: (Echeverria, Rodriguez et al. 2016, Gulich, Zunino 2014, Grech, Mazur 2013). The most recent method (Echeverria, Rodriguez et al. 2016) identifies a transition range for the change in scaling behaviour rather than a point at which change occurs. The second method uses the coefficient of determination (R^2) (Gulich, Zunino 2014) to determine non overlapping segments with the best R^2 values. The different combinations of non-overlapping linear segments are used to infer different scaling regions in the DFA results. The third method introduced by (Grech, Mazur 2013) uses a similar methodology as in the Joinpoint Trend Analysis Software for cancer research (National Cancer Institute 2016) where changes in trends are identified when the probability distribution of the sum of residuals of a piecewise linear fit is significantly different from a piecewise linear fit with one additional segment.

The novelty of the r-DFAn method is that it explicitly determines the statistical significance of adjacent scaling regimes while taking into account the total number of scaling regimes with the help of the multiple comparison procedure as previously explained.

Study site

Description

The study area is located in Wallingford, Oxfordshire, United Kingdom (Figure 5) with a number of gauges installed on the site of the Centre for Ecology and Hydrology (CEH). The Wallingford Observatory comprises two shallow boreholes (WL84 and WL85) screened within shallow alluvial gravel deposits, a stilling well located in the nearby River Thames, and an automatic weather station (AWS). Their locations are shown in Figure 5. The boreholes are sited on a grass verge adjacent to a set of buildings at CEH. The verge is actively managed and cut frequently during the growing season. Several poplar trees (*Populus*) and a sycamore tree (*Acer pseudoplatanus*) are located within 10 m of the borehole. Areas of hard standing, associated with nearby buildings and car parks, limit infiltration at the site. The stilling well is positioned 420 m west of the boreholes and is adjacent to the eastern bank of the River Thames. The AWS lies between the boreholes and stilling well, within cattle pasture.

Geology and hydrogeology

The Wallingford site is located close to a major geological boundary in the course of the River Thames. Upstream from Wallingford, the river flows across a broad, mudstone-floored valley formed from Early Cretaceous Gault Clay (Figure 6). Downstream from Wallingford, the River Thames is progressively constricted as it passes through the Goring Gap which divides the Chiltern Hills and the Berkshire Downs. Here the River Thames flows across the Upper Greensand and the overlying Late Cretaceous Chalk Group. The geological formations are inclined gently toward the southeast so that the river crosses younger formations in a downstream direction.

The Upper Greensand in the Wallingford area is a heterogeneous deposit of mudstones, sandstones and siliceous malmstones and forms an aquifer unit approximately 25 m thick above the Gault Clay (Figure 6). The Upper Greensand is overlain by the West Melbury Marly Chalk, which although forming the base of the Chalk Group, differs markedly from the pure-white, high-porosity carbonates, which form the bulk of the overlying Chalk. The West Melbury Marly Chalk is largely composed of carbonate-rich mudstone (marl) with a distinctive glauconite-rich unit (Glauconitic Marl Member) at the base. This basal part of the Chalk has a low permeability and springs are often seen to emerge from overlying thick-bedded chalks around the flanks of the Chiltern Hills and Berkshire Downs. The spring line is generally located just below the boundary with the overlying Zig Zag Chalk Formation.

The River Thames is separated from the Cretaceous bedrock formations by a layer of Quaternary sand and gravel, which is typically around 5 m thick and can extend across the valley floor for up to 2 km. The sands and gravels are subdivided into a number of named river terrace deposits. The Northmoor Sand and Gravel member occurs beneath and adjacent to the floodplain of the modern River Thames and in the Wallingford area is subdivided into a lower facet and an upper facet. The lower facet is generally concealed beneath a thin (metre-thick) cover of Holocene alluvium.

The Wallingford boreholes were drilled into the upper facet of the Northmoor Sand and Gravel on a minor terrace just above the level of the modern Thames floodplain. They proved 0.5 m of soil, overlying 4.0-4.2 m of interbedded sandy gravel and gravelly sand with fine to coarse pebbles composed largely of limestone, ironstone and flint. The gravels rest sharply on grey mudstones of the Glauconitic Marl. This low permeability horizon at the base of the Chalk Group hydraulically isolates the highly permeable sands and gravels from the underlying Upper Greensand aquifer. There is a hydraulic head difference of around 4 - 5 m between this aquifer and the overlying terrace sand and gravels, with the potentiometric head of the Upper Greensand typically above ground level during the winter.

Hydrology

The River Thames is the most prominent surface water feature traversing the sands and gravels with a mean flow and baseflow index (BFI) of 28.3 m^3/s and 0.64, respectively, as monitored 8 km upstream at Day's Weir (Marsh, Hannaford 2008). The River Thame is the most significant local tributary of the Thames, with the confluence 6.5 km upstream of the site. The Thame has a mean flow of 3.8 m^3/s and BFI of 0.59 at Wheatley (51.740^o N 1.115^o W). Ewelme Brook is an example of one of the smaller groundwater dominated streams seen locally which emerge as springs from the top units of the West Melbury Chalk, and flow across the sands and gravels before converging with the Thames. It has a mean flow and BFI of 0.05 m^3/s and 0.98, respectively, 400 m downstream of its source (51.620^o N 1.074^o W). The mean annual rainfall recorded between 1972 and 2007 in Wallingford is 596 mm.

Data Collection and Inspection

Data Collection

The six datasets discussed herein are river stage, groundwater levels, river temperature, groundwater temperature, rainfall and air temperature. Details of the datasets and gauge installation are summarised in Table 1 and Table 2 respectively.

Groundwater levels and temperature are monitored using a 3.5 mH_2O range MEAS KPSI^{TM} 501 pressure transducer in borehole WL84. The sensors are located 4.5 m below ground level adjacent to the screen for representative groundwater temperature measurements. (Sorensen, Butcher 2011) reported this was the most accurate pressure transducer (Transducer F) out of sixteen models tested with an accuracy in field tests of ± 4 mm and no evidence of drift. An additional 3.5 mH_2O range MEAS KPSI™ 500 pressure transducer is also installed within the borehole to validate the primary dataset. Temperature on both KPSI™ sensors is typically accurate to ± 0.1°C, but specified to within ± 0.25 °C. All measurements are recorded every minute and telemetered using Adcon A723 addITs.

In borehole WL85, a 3.5 m range In-Situ Inc. Level TROLL® 500 is installed and logging at a 1 minute frequency. This sensor is specified as accurate to ± 3.5 mm by the manufacturer. This dataset provides a backup dataset in the event of transducer or telemetry failure at borehole WL84.

Frequent manual observations of groundwater level are undertaken at both boreholes with a dip tape to detect any evidence of instrument malfunctioning or drift (Post, Asmuth 2013). The dip tape is regularly calibrated against an EU Class I measuring tape, which has a tolerance of ± 0.4 mm over the length used.

At the stilling well, river stage and temperature were measured at 1 minute interval with a 3.5 mH_2O range MEAS KPSI™ 500. There is currently no backup sensor installed at this location.

Meteorological variables are monitored every 15 minutes using a Didcot AWS, with DICo Probes for air temperature. The temperature is typically accurate to ± 0.1 °C, although calibrated to an accuracy of ± 0.2 °C. Rainfall is monitored with a tipping bucket rain gauge (0.2mm tip volume), which is mounted at ground level to reduce the effects of undercatch (Rodda and Dixon, 2012).

Data quality control

The groundwater and river datasets span 2,101,873 records from 08:48 2nd January 2012 until 00:00 01st January 2016. These datasets contained missing values, which totalled 1.0 and 0.7 % of the total record lengths in the borehole and stilling well, respectively. These were infilled using four techniques (Table 3). The datasets contained several small gaps (<10 min), including numerous 1 minute gaps, for example the groundwater level dataset contains 393 records. These records were all infilled via linear interpolation, which is considered reasonable over such short timeframes.

The majority of groundwater level data infilling was via linear regression with borehole WL85 (R^2 = 1.00 from 616482 concurrent records). However, over 33 hours in June 2013 there was no corresponding record from WL85. Therefore, the rate of change over the preceding 24 hour period was used to reconstruct the groundwater level data. This enabled anticipated short-term fluctuations to be captured in the absence of any precipitation. This was not thought to have a significant impact on the results, as the infilled time is less than 0.25% of the entire time period. Linear interpolation over periods in excess of 10 minutes was used for the groundwater temperature and river datasets.

There was no evidence of drift noted in the WL84 groundwater level dataset. This was confirmed via comparison with manual level observations which showed no deterioration in accuracy with time, with all data within ± 3 mm. Furthermore, there was no systematic deviation in readings between the pressure transducers within borehole WL84.

Both air temperature and rainfall datasets contained missing values totalling 10% in record length, notably 3516 records between 13th November and 20th December 2013 and 4700 records between 24th December 2014 and 11th February 2015. These were infilled with hourly data from Benson located 2 km northeast of Wallingford and is indicated in Figure 5. Benson temperature data were downscaled to 15 minute using linear interpolation, then used to infill the Wallingford data. Rainfall data were not downscaled, and were not adjusted for location as 88 % of the concurrent hourly totals were identical.

Data Inspection: Processes and time-scales

Rainfall was highly unusual during the study period, exceeding the average in 2012 and 2014 by about 40 and 50% respectively, and approximately equal to the average in 2013 and 2015 by about 3 and -5% respectively. However, during early 2012 Southern Britain had actually been experiencing drought conditions. In April, though, there was an abrupt change in the weather pattern across the UK, which preceded unprecedented rainfall locally (Parry, Marsh et al. 2013). This resulted in atypical river flows during late spring and summer and, moreover, inhibited the development of soil moisture deficits during summer 2012. Consequently, the onset of runoff was rapid during the winter rains causing periods of high flow throughout October 2012 – April 2013 along the Thames. The summer of 2013 was reasonably warm and dry and resulted in high soil moisture deficits developing. However, the clustering of deep depressions throughout December 2013 and January 2014 produced high rainfall, high runoff and the highest average January flow along the Thames since records began in 1883 (CEH/Met Office, 2014).

Groundwater head remains elevated above the river stage throughout the period indicating the potential for perennial groundwater discharge to the Thames (Figure 7). The elevated groundwater head could be supported through upwelling from the Chalk to the East or the Upper Greensand to the West where the overlying Glauconitic Marl Member is absent. Other contributions could originate via loses from upgradient surface waters, such as the River Thame or more groundwater dominated streams like Ewelme Brook.

Rises in River Thames stage are a response to flow from upstream catchments and hence are much greater than concomitant rises in groundwater head (Figure 7). The River Thames response would be a combination of both groundwater discharge and overland flow which is likely to occur north of the piezometer site, where the river and its tributaries flow across the impermeable Gault Clay Formation.

Groundwater temperature is relatively stable displaying a low-amplitude sinusoidal pattern which peaks in October and reaches its minima in April (Figure 7). These peaks and troughs are lagged in comparison to air temperature. By contrast, river temperature responds quickly to air temperature throughout, but without the same extremes because of the higher thermal capacity of water.

It is observed that there can be a marked and rapid rise in borehole water level during and shortly after intense rainfall events (Figure 8 and Figure 9). This is believed to be due to the Lisse effect, which arises from air entrapment during these events, particularly during summer. Figure 9 shows the response of the borehole water level to individual rainfall events during August (a summer month) where the Lisse effect is clearly observed and during November-December (winter months) where the Lisse effect is less prominent. The Lisse effect tends to occur in shallow unconfined riparian aquifers similar to the that studied here (Weeks 2002). During these changes in level there are also concurrent changes in groundwater temperature (Figure 9). Figure 9 captures one such event. Initial change in groundwater temperature (marked as 'local minimum' in Figure 9) is attributed to initial inflow of groundwater with a slightly different ambient temperature into that in the well during the initial rise in the borehole water column. This is followed by a reversal in the temperature gradient which occurs due to mixing of the water column in the well. The mixing is believed to be induced by turbulence due to the rapid inflow and then outflow of water as a result of the build-up and then reduction of air pressure in the unsaturated soil during the Lisse effect. This results in a local temperature maximum occurring during the declining phase in the borehole water level. The temperature then starts to transition into a new equilibrium state after the dissipation of the Lisse effect. When such events occur during the winter an inverse response occurs with an initial local maximum followed by a larger local minimum. The observed rise in groundwater level in Figure 9 is ~0.15 m in response to a rain event that had a cumulative depth of ~0.01 m. With a specific yield estimate of about 0.15 for the study site, the observed rise in groundwater level is expected not to exceed 0.07 m. And hence the 0.15 m rise in groundwater level for this event is evidently caused by the Lisse effect.

Controls on river and groundwater levels are diurnal and seasonal. During the summer, river levels in the stilling well are noticeably influenced by bow waves emanating from passing boat traffic. This can result in random noise of several millimetres during daylight hours (Figure 8a). Such noise is less pronounced during the winter months, and also tends to be focussed during weekends or public holidays.

Evapotranspiration from groundwater storage is similarly diurnal and seasonal producing daytime drawdown and overnight recovery typically between April and October (Figure 10). It is likely to be a consequence of the nearby poplar trees which have been observed to root to at least 3.2 m below the surface (Heilman, Ekuan et al. 1994) and could, therefore, tap the saturated zone directly.

Contributions from the sycamore are likely to be more limited as the species tends to restrict root growth to within the top metre (Heilman, Norby 1998, Simon, Collison 2002).

Results and discussion

The Lisse effect – which was explained under the Data Inspection Section – is an artefact of the monitoring well's response to heavy rainfall events and is not, therefore, indicative of a physical increase in groundwater storage. Hence, as suggested by (Zhang, Gong et al. 2011) the data will be corrected for the Lisse effect. The procedure developed for the removal of the Lisse effect is detailed in Appendix A. Both groundwater level and temperature data will be corrected for the Lisse effect and fractal behaviour for both observed and corrected time series will be presented.

Figure 11 to Figure 14Figure 14 present the results of r-DFAn for all the datasets listed in Table 1. Table 4 presents a summary of the global scaling exponents and persistent crossovers in r-DFA1 for all datasets.

The Lisse effect has a noticeable effect on the mono-fractal behaviour of groundwater temperature and levels (Figure 11 and Figure 12), particularly at intermediate time scales (i.e. around 1000 mins or 0.7 days). Where, in the case of the borehole water level, correction for the Lisse effect removes a crossover, due to the reduction in $F(L)$, at these intermediate time scales. The global fractal exponents for groundwater temperature with and without the Lisse effect are ∼1.43 and ∼1.40 respectively, and that for groundwater levels are ∼1.68 and ∼1.78 respectively. Hence, the global scaling behaviour is not strongly affected by the existence of the Lisse effect.

Global fractal behaviour of rainfall, river stage and groundwater level (corrected for Lisse effect) at the Wallingford site are consistent with previous studies (Matsoukas, Islam et al. 2000, Li, Zhang 2007) where rainfall is similar to white noise ($\propto = 0.5$) and river stage and groundwater fluctuation is more structured and tends to Brown noise ($\propto = 1.5$). Here, the global scaling exponent for rainfall, river stage and groundwater level are ∼0.72, ∼1.60 and ∼1.78 respectively (Figure 13-E, Figure 13-F and Figure 13-G). (Little, Bloomfield 2010, Li, Zhang 2007, Zhang, Schilling 2004) speculate on the role of runoff, recharge and the carrying medium i.e. soil, on altering the fluctuation structure of rainfall to produce more structured fluctuation in groundwater level and river stage.

Crossovers are observed in all datasets studied. Notable is the protuberant shape observed for air temperature (Figure 13-A), groundwater temperature (Figure 13-C), and river temperature (Figure 13-D) with maximum bulge for r-DFA1 at around ~14 hours, ~11 hours and ~9 hours respectively. Persistence of this crossover across higher order r-DFAn indicates a strong presence of a periodic cycle with a cycle length smaller than that observed in r-DFA1 at the maximum bulge (Li, Zhang 2007, Sadegh Movahed, Jafari et al. 2006, Kantelhardt, Koscielny-Bunde et al. 2001). The degree of protuberance in the fractal domain is proportional to the amplitude of the cycle in the time domain (which is presented in Figure 4).The amplitude of the cycle in Figure 4 is related to the degree of protuberance in that the degree of protuberance for air temperature is larger than that for river temperature and which in turn is larger than that for groundwater temperature.

An important speculation that relates the r-DFAn results of the three temperature time series and the three hydrological time series (i.e. rainfall, groundwater levels and river stage) is the degree of similarity of the DFA results of the former compared to that of the latter. The similarity of r-DFA results of the three temperature time series (i.e. air temperature, river temperature and groundwater temperature), is attributed to the underlying dominantly-linear heat transfer process that does not induce or alter the fractal properties of the temperature time series. However, the DFA results of rainfall, river stage and groundwater levels do not exhibit the same degree of similarity due to underlying non-linear recharge, runoff and baseflow transfer functions.

The rainfall series has one persistent crossover at 1.6 days for r-DFA1. Investigation of the rainfall series in the time domain revealed that all storms last for a maximum period of 1.4 days and about 75% of dry period length (i.e. dry periods between storms) are shorter than 1.6 days; Storms were estimated by clustering non-zero rain with no longer than 2 hours of dry period as was done in (Ireson, Butler 2011)). Keeping these estimates in mind, it is speculated that the 1.6 days crossover separates between two regimes where the first regime, that corresponds to scales smaller than 1.6

days, is affected by the intermittency of rainfall. The second regime, that corresponds to scales from 1.6 days to a number of months, is no longer dominated by the effect of storms and rain events. Published results for rainfall do not coincide with the rainfall series at Wallingford. One such case are the rainfall series studied in (Matsoukas, Islam et al. 2000) from 9 different locations in the US. A crossover between 5 and 10 days was observed at the 9 locations and its occurrence was related to the separation between meteorological and climatological regimes that act as forcing on the rainfall time series. However, the scaling exponents before and after the crossover coincide with our findings where a SE of about 1.0 is observed at smaller scales and a SE of about 0.6 is observed at larger scales. In another publication, (Tessier, Lovejoy et al. 1996) observed a crossover at about 16 days for rainfall time series collected from 30 different catchments in France. (Koscielny-Bunde, Kantelhardt et al. 2006) studied daily rainfall data from various places across the world, hence, it is only the scaling exponents on larger scales that can be compared. The scaling exponents from Wallingford and those reported in (Koscielny-Bunde, Kantelhardt et al. 2006) are similar because both are close to white noise as opposed to 1/f noise that is exhibited across smaller scales in the Wallingford 15-minute rainfall data.

The fractal behaviour of river stage (Figure 13-F) and groundwater levels (Figure 13-G) are very similar. (Li, Zhang 2007) speculated the effect that river stage fractal properties would have on that of groundwater levels, especially at the larger scales. However, River Thames, which is generally groundwater dominated (with a BFI of 0.64 measured 8 km upstream of the site), is expected to have fractal properties similar to that of groundwater fluctuation.

(Little, Bloomfield 2010), as reported in (Labat, Masbou et al. 2011), studied GW levels and found that they exhibited scaling exponents ranging from 1.20 to 1.65. (Li, Zhang 2007) reported two crossovers; one between a few days and 10 days and the second was between a few months and a year. Unfortunately, the groundwater scale ranges studied herein are different from those studied in (Li, Zhang 2007), hence a comparison is not possible. However, according to (Yu, Ghasemizadeh et al.

2016), the fractal behaviour of groundwater levels is found to be site specific and hence need not be similar.

Finally, Figure 14 summarises all crossovers that persist across all r-DFA orders in the 6 datasets studied. As explained earlier when illustrating r-DFAn on the synthetic signal, due to anticipated interaction between the different scaling regimes, the 'true' crossover is expected to fall before the crossover in r-DFA1. Evidently, the crossovers in all datasets (except for the second CO in the groundwater levels dataset) follow a generally linear trend. Noteworthy is the similarity of slopes of the three unaltered temperature time series (air temperature, river temperature and groundwater temperature) that the crossovers follow. In addition, the slopes for river stage and the first CO of groundwater levels are of similar magnitude.

Summary and conclusions

The fractal behavior of six very high-resolution datasets was investigated using robust detrended fluctuation analysis procedure (r-DFAn) that allows for accurate non-subjective determination of global scaling exponents and statistically significant changes in the scaling regimes (crossovers). The datasets investigated were 1-minute river and groundwater temperature and levels, 15-minute rainfall and temperature. The variables were collected in Wallingford, UK, over a period of 4 years. The study site is formed of a shallow gravel aquifer that drains into River Thames. Detailed inspection of all variables in the time domain was presented along with their fractal behavior. Due to the very high resolution of the data collected and the high permeability of the aquifer, the Lisse effect was identified. Insights into the dynamics taking place inside the groundwater monitoring well were inferred from a combined inspection of the one-minute groundwater level and groundwater temperature data. Plant root uptake was clearly identified in the groundwater level time series with recession during the day and infiltration during the night. The removal of the Lisse effect from the affected time series showed how the Lisse effect influences the fractal behavior of these time series at intermediate time scales (at about one day).

The high resolution of the data enabled the study of their mono-fractal behavior from a time scale as short as 3 minutes for 1-minute river and groundwater data and a time scale of 45 minutes for the 15-minute meteorological data. At these scales, the river stage and groundwater levels exhibit a strong and persistent crossover at sub-hourly time scales which would not be detected with coarser-resolution time series.

As for the temperature time series, the periodicity, which is observed in the time series of the air, river and groundwater temperature series, was clearly captured in the fractal analysis in the form of a protuberant shape with a size proportional to the amplitude of the periodicity observed in the time domain. We believe that the underlying (dominantly) linear process of temperature conductance has led to an 'approximately linear' transfer of fractal behavior between the temperature series whereas the underlying non-linear transfer processes of runoff and infiltration that rainfall undergoes did not lead to the same degree of similarity in fractal behavior of rainfall, river stage and groundwater fluctuation.

The fractal behaviour of all datasets was presented, however, a model is required in order to be able to ascertain the driving forces that cause the observed fractal behaviour. The role of soil in acting as a 'fractal filter' of water along its path way, and the role of the processes of recharge and base flow on the fractal properties of rainfall, is a concept that, to the best of our knowledge, is not yet well established. The degree to which models are able to capture fractal behavior of hydrological and hydro-geological time series is an area worth investigation, in light of recent successful attempts like that of (Williams, Pelletier 2015) and (Russian, Dentz et al. 2013).

Acknowledgment

Abrar Habib is affiliated with the University of Bahrain which sponsors her Doctoral Research at Imperial College London.

James Sorensen, Dr John P Bloomfield, and Dr Andrew J Newell publish with the permission of the Executive Director of the British Geological Survey (NERC).

Figures and Tables

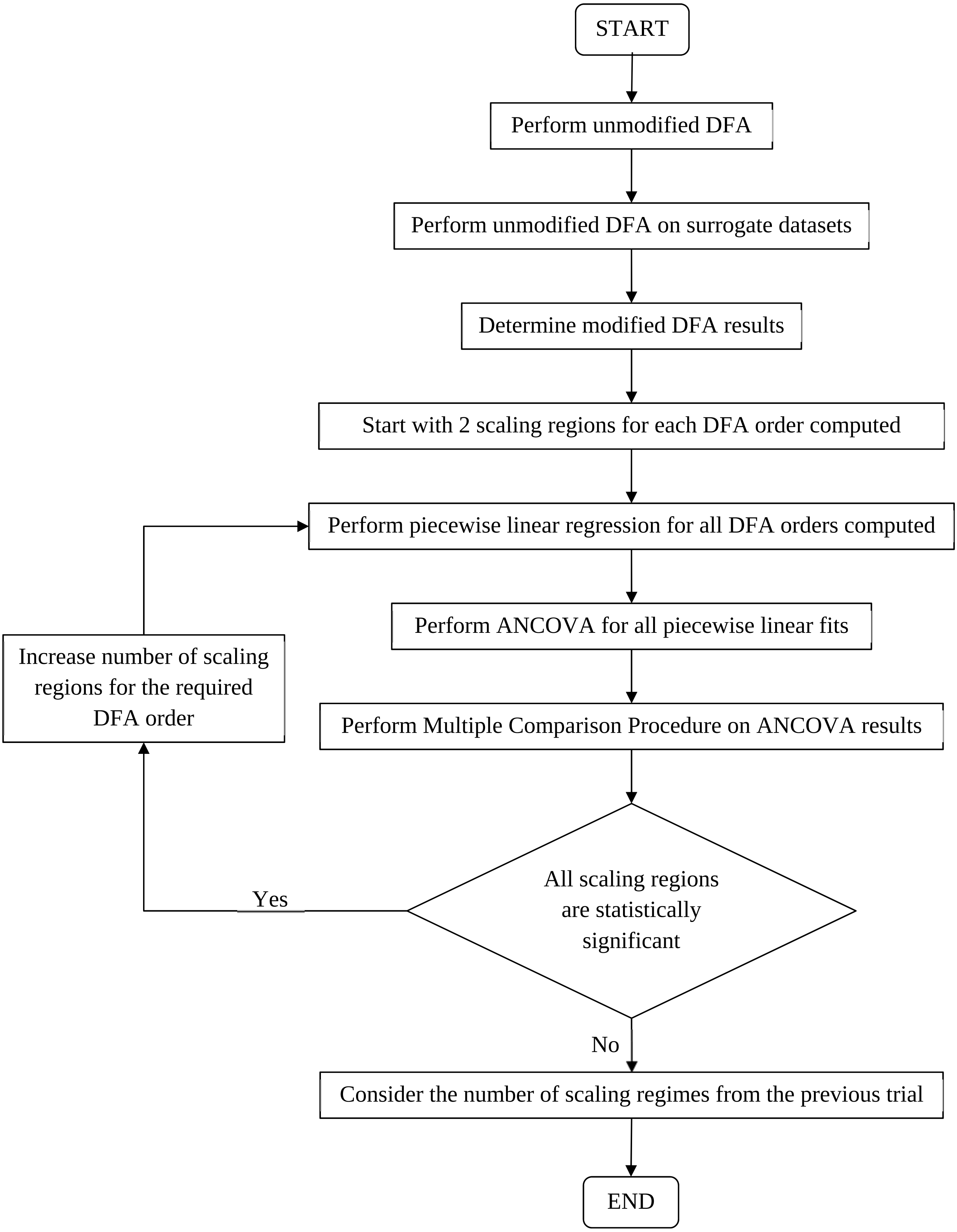

Figure 1 Flowchart of r-DFAn procedure

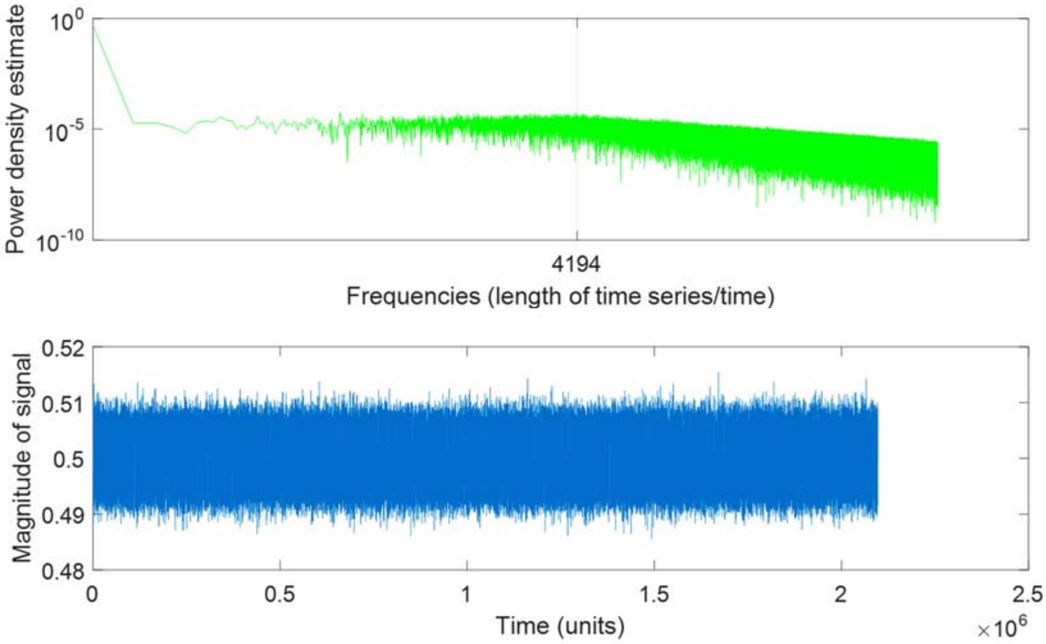

Figure 2 Mono-Fractal signal in frequency (top panel) and time (bottom panel) domains with change in the scaling regime at a frequency corresponding to 500 units (indicated with a grey line).

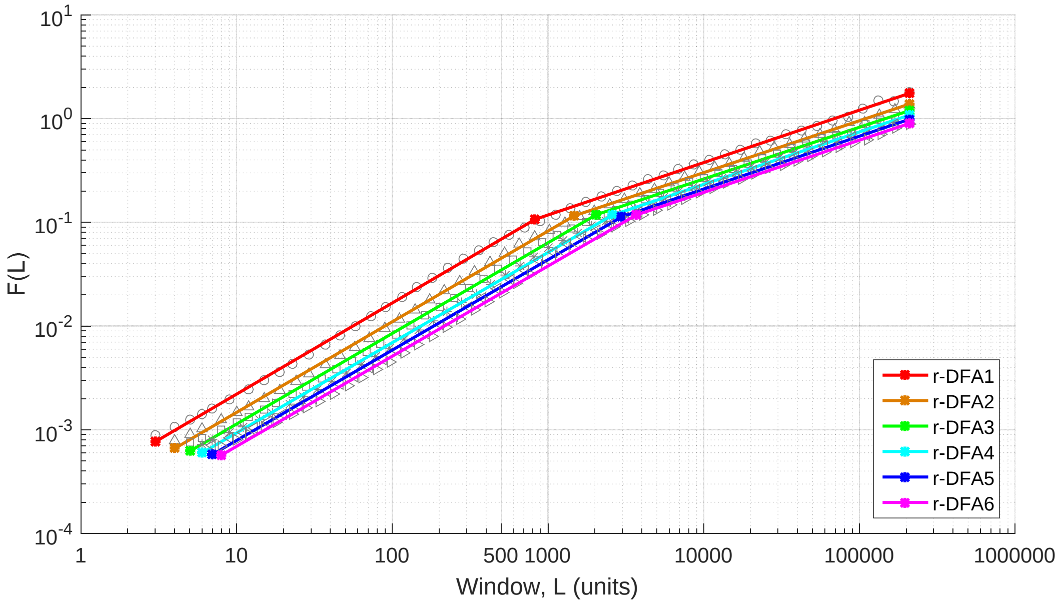

DFA order	Global SE	SE 1	SE 2	CO 1
1	0.70	0.879	0.506	827
2	0.71	0.874	0.500	1475
3	0.72	0.873	0.500	2044
4	0.73	0.870	0.505	2592
5	0.74	0.872	0.509	2983
6	0.74	0.869	0.503	3982

Figure 3 r-DFA of synthesized mono-Fractal time series of length 221 data points, a theoretical crossover at 500 units and a theoretical scaling exponent of 1.0 before crossover and 0.5 after the crossover.

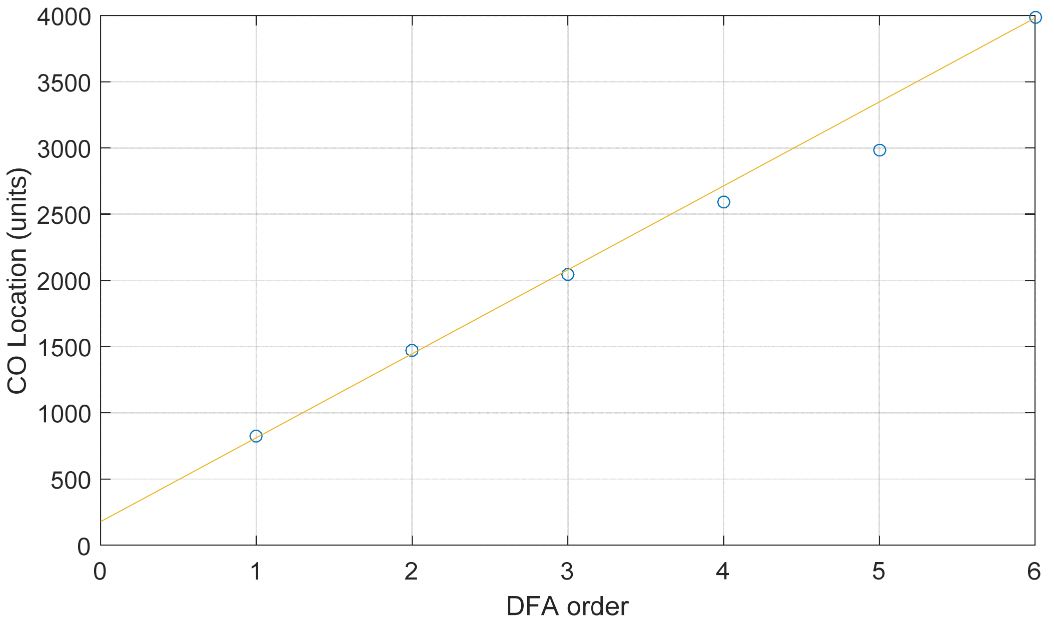

Figure 4 Summary of COs of the synthetic mono-fractal signal with change in scaling regime

Figure 5 Illustration of Wallingford study site location and relevant gauges from Google Earth

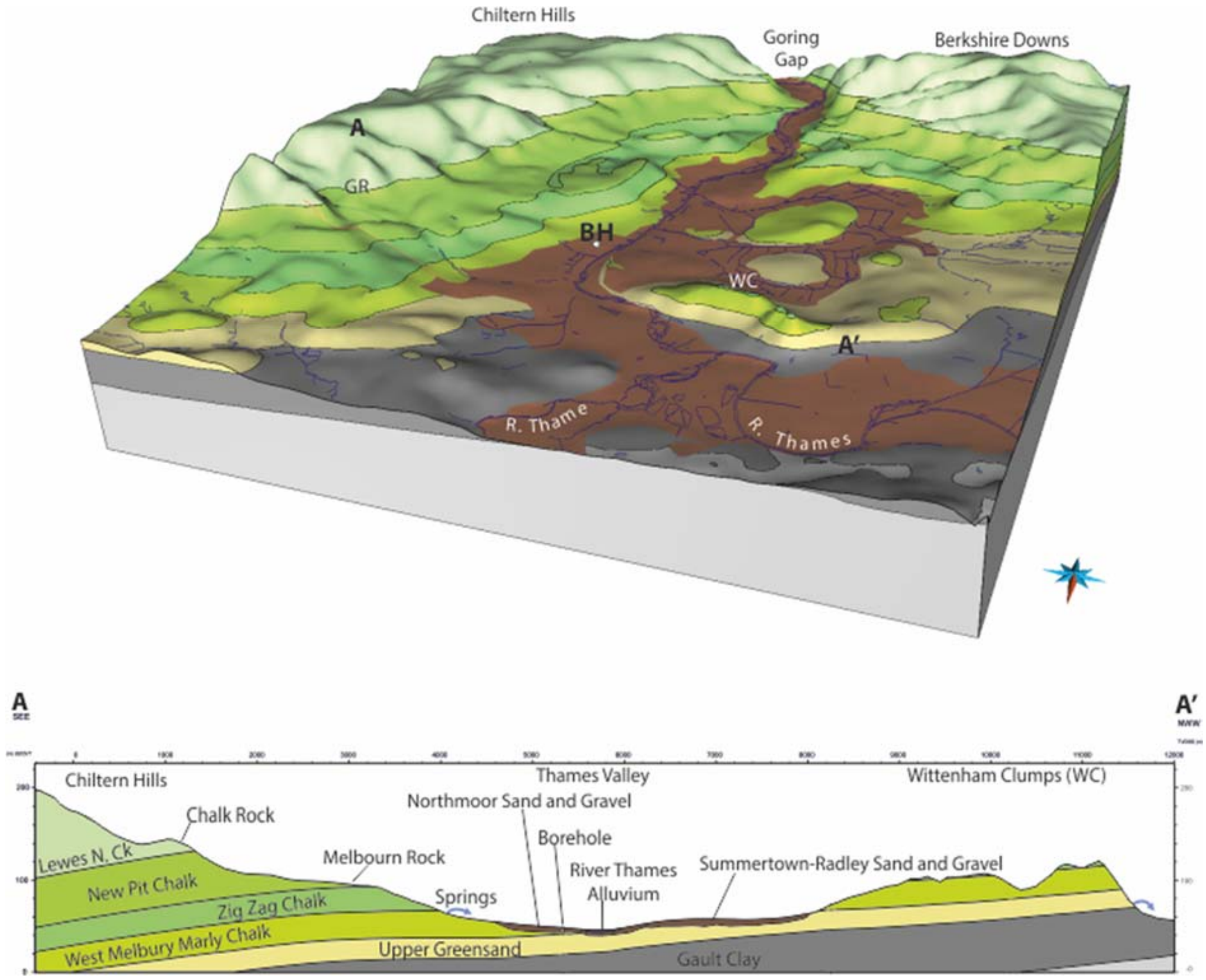

Figure 6 Block diagram showing the topography and geology surrounding the borehole site. Block covers an area of approximately 16x17 km and is viewed looking south (downstream) toward the Goring Gap. The block covers an altitudinal range of 360 m and is viewed with a vertical exaggeration factor of X10. See cross-section (b) for a key to the colours of the geological formations and abbreviations.

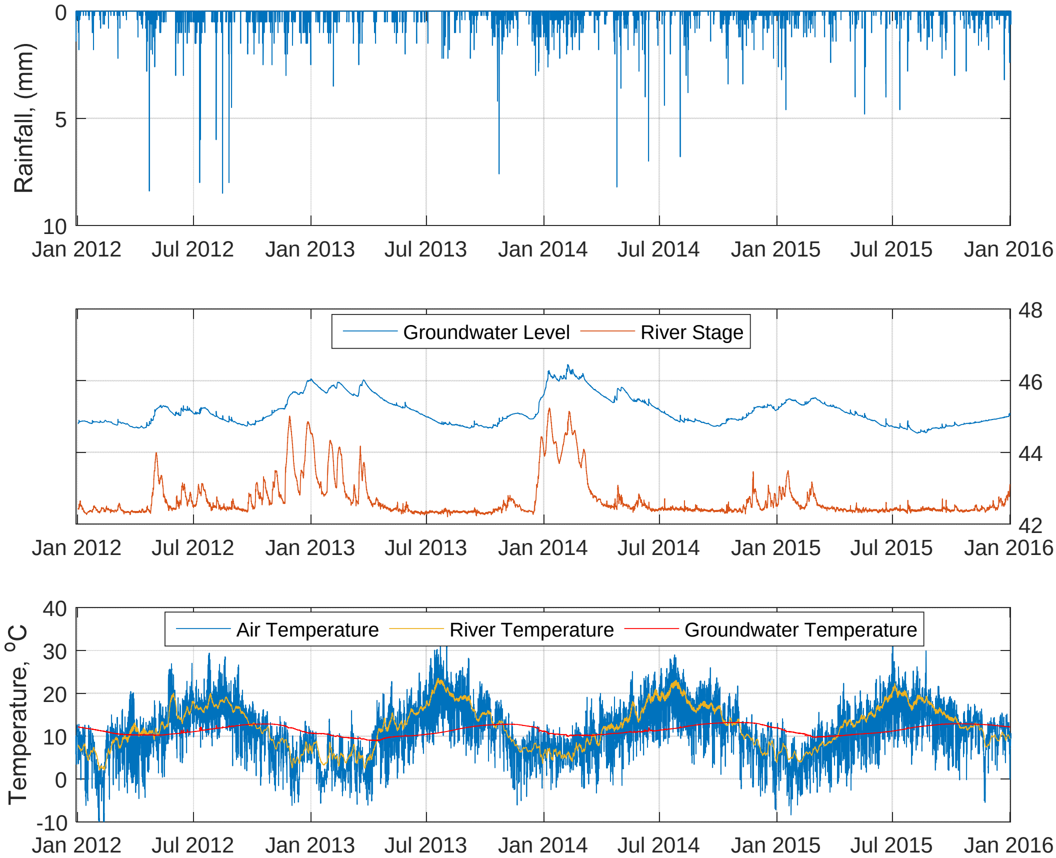

Figure 7 Full time series of daily rainfall, river and groundwater level, and air, river and groundwater temperature.

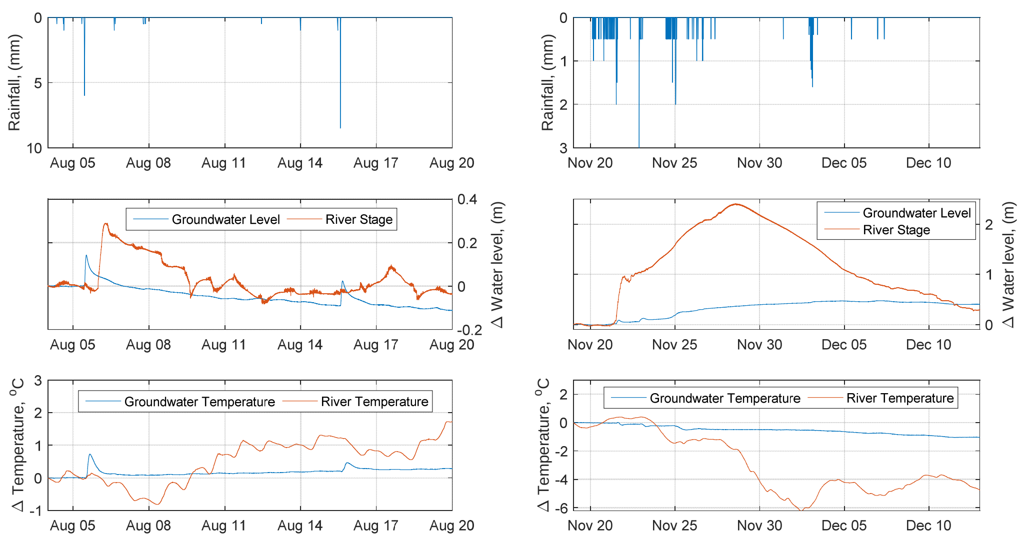

Figure 8 Response of river and groundwater levels and temperature to events in (a) Left panel: August 2012 (b) Right panel: November 2012

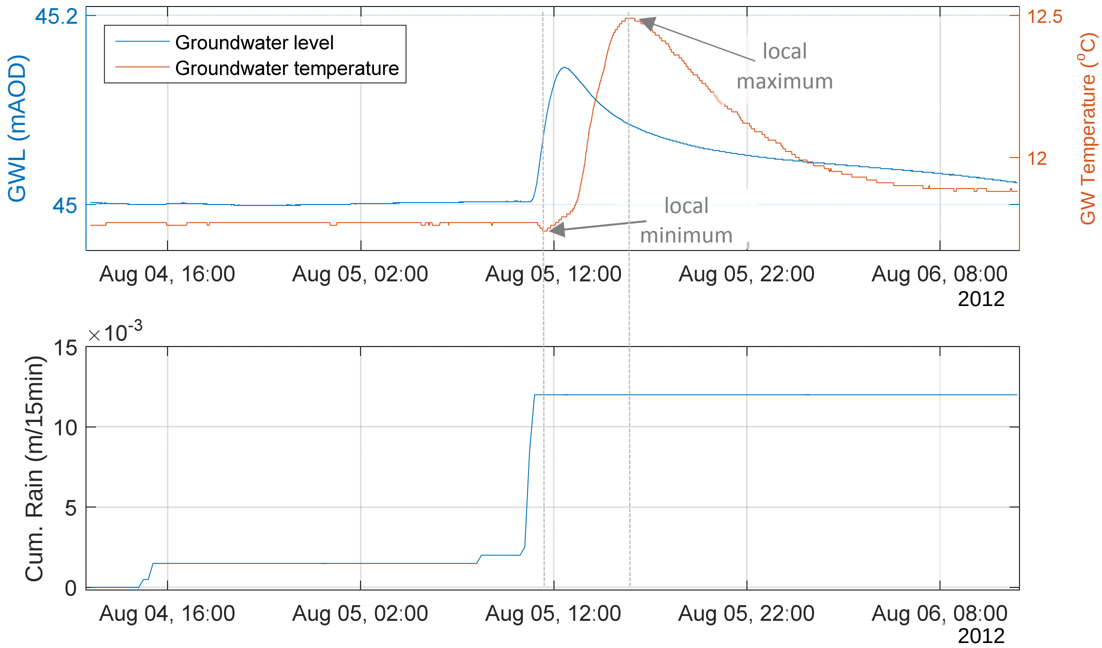

Figure 9 Top panel: Groundwater level and temperature with focus on one Lisse event (grey dotted lines mark minimum and maximum groundwater temperature differences); Bottom Panel: Coinciding cumulative rainfall.

Figure 10 Groundwater level at Wallingford exhibiting diurnal fluctuation due to plant root uptake during daytime

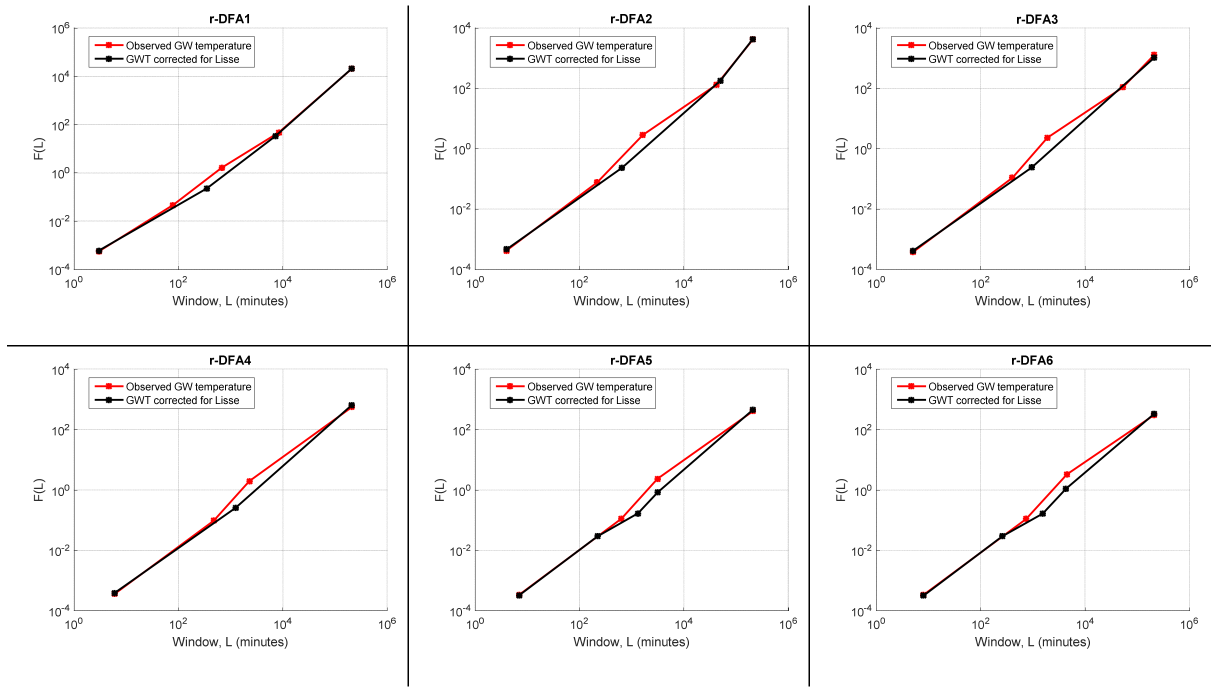

Figure 11 Illustration of the effect of the Lisse effect on the fractal behaviour of Groundwater temperature

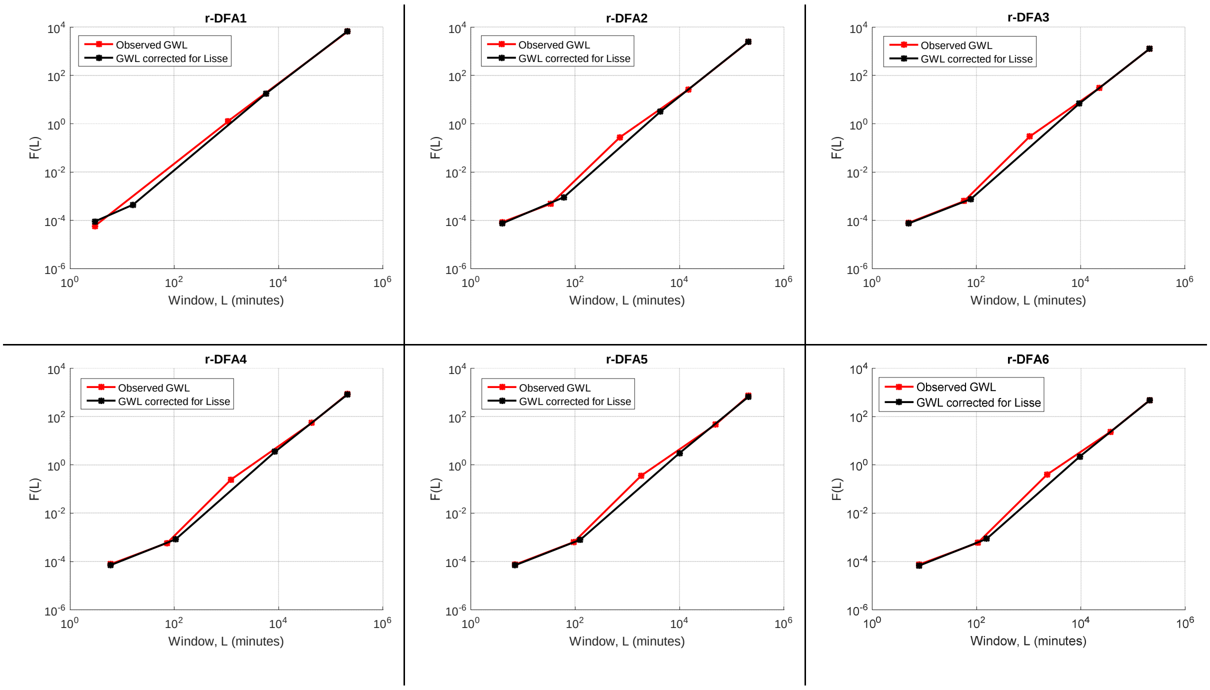

Figure 12 Illustration of the effect of the Lisse effect on the fractal behaviour of Groundwater level

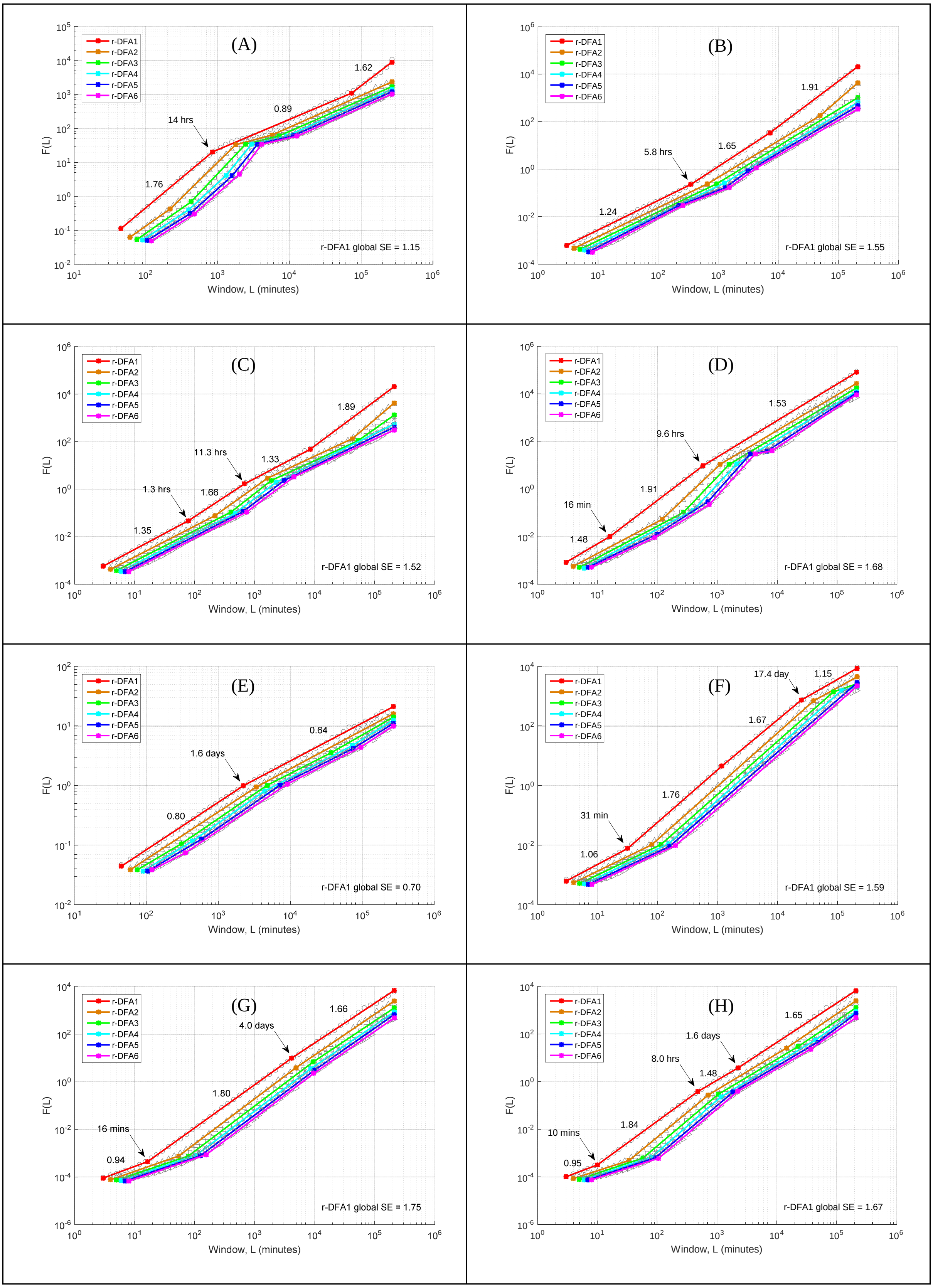

Figure 13 r-DFAn results of (A) dry air temperature, (B) 1-minute groundwater temperature corrected for Lisse effect, (C) 1-minute observed groundwater temperature, (D) 1- minute river temperature, (E) 15-minute rainfall intensity, (F) 1-minute river stage, (G) 1-minute groundwater level corrected for Lisse effect, and (H) 1-minute observed groundwater level

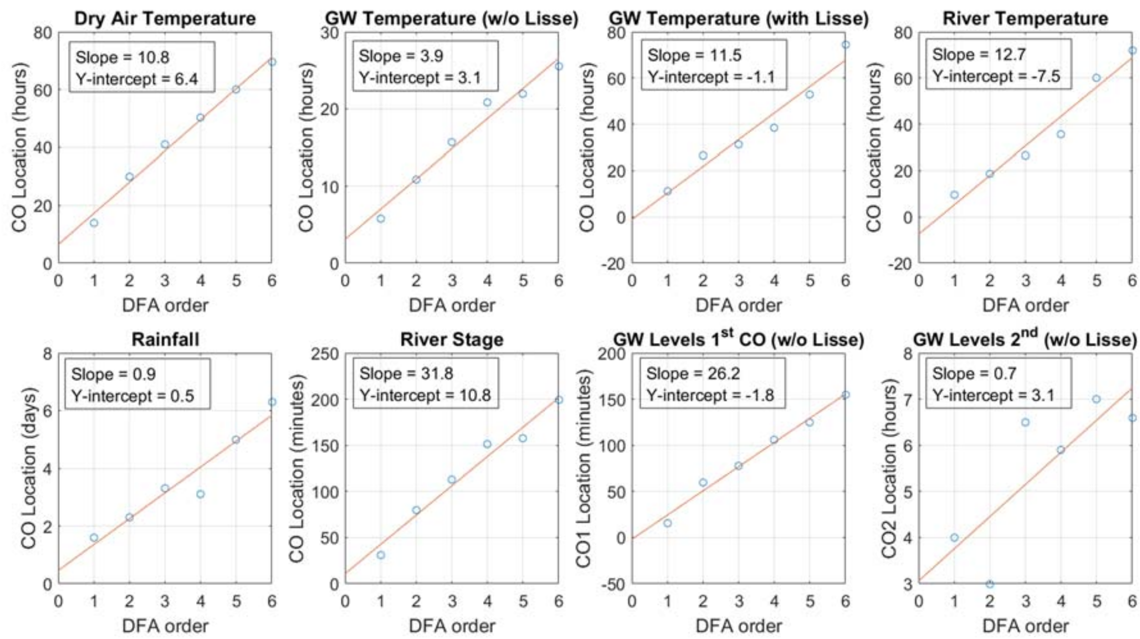

Figure 14 Summary of COs that persist through all orders of DFA for all datasets studied

Table 1 All datasets analysed for fractal behaviour

Dataset	Resolution (minutes)	Data length
Dry air temperature	15	01/2012 to 12/2015
River Thames temperature Wallingford	1	01/2012 to 12/2015
Groundwater temperature at Wallingford (with and without the Lisse effect)	1	01/2012 to 12/2015
Rainfall at Wallingford	15	01/2012 to 12/2015
River stage at Wallingford	1	01/2012 to 12/2015
Groundwater levels at Wallingford (with and without the Lisse effect)	1	01/2012 to 12/2015

Table 2 Details of installations

Installation	Latitude (°)	Longitude (°)	Elevation (mAOD)	Total depth (m)	Screen (mBGL)
WL84	51.6036	-1.1107	47.883	5.01	2.17 - 4.71
WL85	51.6036	-1.1106	47.778	4.79	1.95 - 4.49
Thames stilling well	51.6047	-1.1164	43.747	N/A	N/A
AWS				N/A	N/A

Table 3 Data infilling and data flags

Data flags	Infilling technique	Groundwater		Thames	
		Level	Temp	Level	Temp
1	None	2050767	2050729	2054175	2054217
2	Linear interpolation (<10 min)	1173	1189	901	902
3	Linear regression	8281	256	93	50
4	Duplication of preceding record	1991	0	0	0
5	Linear interpolation (>10 min)	0	10038	7043	7043

Table 4 Summary of r-DFA results for all the time series analysed

Dataset	Resolution	r-DFA1			
		Global SE	CO 1	CO 2	CO 3
Air Temperature	15 min	1.15	-	14 hr	-
GW Temperature (observed)	1 min	1.52	78 min	11 hr	-
River Temperature	1 min	1.68	16 min	9.6 hr	-
Rainfall Intensity	15 min	0.80	-	-	1.6 day
GWL (observed)	1 min	1.67	10 min	8 hr	1.6 day
River Stage	1 min	1.59	31 min	-	17.4 day
GW Temperature (no Lisse)	1 min	1.55	-	5.8 hr	-
GWL (no Lisse)	1 min	1.75	16 min	4.0 hr	-

References

ALVAREZ-RAMIREZ, J., ECHEVERRIA, J.C. and RODRIGUEZ, E., 2011. Temporal variations of long- term correlations in seismic activity fluctuations. *Physica A: Statistical Mechanics and its Applications,* .

CARAIANI, P., 2012. Evidence of Multifractality from Emerging European Stock Markets (Multifractality Stock Markets). *PLoS ONE,* **7**(7), pp. e40693.

CHEN, F., TIAN, K., DING, X., MIAO, Y. and LU, C., 2016. Finite- size effect and the components of multifractality in transport economics volatility based on multifractal detrending moving average method. *Physica A: Statistical Mechanics and its Applications,* **462**, pp. 1058-1066.

CHEN, Z., IVANOV, P.C., HU, K. and STANLEY, H.E., 2002. Effect of nonstationarities on detrended fluctuation analysis. *Phys.Rev.E,* **65**(4), pp. 041107.

CONDON, L. and MAXWELL, R., 2014. Groundwater-fed irrigation impacts spatially distributed temporal scaling behavior of the natural system: a spatio-temporal framework for understanding water management impacts. *Environmental Research Letters,* **9**(3), pp. 034009.

DAGDUG, L., ALVAREZ-RAMIREZ, J., LOPEZ, C., MORENO, R. and HERNANDEZ-LEMUS, E., 2007. Correlations in a Mozart's music score (K-73x) with palindromic and upside-down structure. *Physica A: Statistical Mechanics and its Applications,* **383**(2), pp. 570-584.

ECHEVERRIA, J.C., RODRIGUEZ, E., AGUILAR-CORNEJO, M. and ALVAREZ-RAMIREZ, J., 2016. Linear combination of power-law functions for detecting multiscaling using detrended fluctuation analysis. *Physica A: Statistical Mechanics and its Applications,* **460**, pp. 283-293.

EICHNER, J.F., KOSCIELNY-BUNDE, E., BUNDE, A., HAVLIN, S. and SCHELLNHUBER, H.-., 2003. Power-law persistence and trends in the atmosphere: A detailed study of long temperature records. *Physical Review E,* **68**(4), pp. 046133.

FRAEDRICH, K. and LARNDER, C., 1993. Scaling regimes of composite rainfall time series. *Tellus A,* **45**(4), pp. 289-298.

GELHAR, L.W., 1974. Stochastic analysis of phreatic aquifers. *Water Resources Research,* **10**(3), pp. 539-545.

GRECH, D. and MAZUR, Z., 2013. On the scaling ranges of detrended fluctuation analysis for long-term memory correlated short series of data. *Physica A: Statistical Mechanics and its Applications,* **392**(10), pp. 2384-2397.

GULICH, D. and ZUNINO, L., 2014. A criterion for the determination of optimal scaling ranges in DFA and MF-DFA. *Physica A: Statistical Mechanics and its Applications,* **397**, pp. 17-30.

HABIB, A., 2016. *Robust detrended fluctuation analysis (r-DFAn) (File ID: 60026).*

HEILMAN, P.E., EKUAN, G. and FOGLE, D., 1994. Above- and below-ground biomass and fine roots of 4-year-old hybrids of Populus trichocarpa x Populus deltoides and parental species in short-rotation culture. *Canadian Journal of Forest Research,* **24**(6), pp. 1186-1192.

HEILMAN, P. and NORBY, R.J., 1998. Nutrient cycling and fertility management in temperate short rotation forest systems. *Biomass and Bioenergy,* **14**(4), pp. 361-370.

HENNIG, H., FLEISCHMANN, R., FREDEBOHM, A., HAGMAYER, Y., NAGLER, J., WITT, A., THEIS, F.J. and GEISEL, T., 2011. The Nature and Perception of Fluctuations in Human Musical Rhythms (Nature of Fluctuations in Human Musical Rhythms). *PLoS ONE,* **6**(10), pp. e26457.

HU, J., GAO, J. and WANG, X., 2009. Multifractal analysis of sunspot time series: the effects of the 11-year cycle and fourier truncation. *Journal of Statistical Mechanics: Theory and Experiment,* (02), pp. P02066.

HU, K., IVANOV, P.C., CHEN, Z., CARPENA, P. and STANLEY, H.E., 2001. Effect of trends on detrended fluctuation analysis. *Physical review.E, Statistical, nonlinear, and soft matter physics,* **64**(1), pp. 011114.

HURST, H.E., 1951. Long-term storage capacity of reservoirs. *American Society of Civil Engineers Transactions,* , pp. 770.

HURST, H.E., 1956. Methods of using long-term storage in reservoirs. *Institution of Civil Engineers,* **5**(5), pp. 519-543.

IRESON, A.M. and BUTLER, A.P., 2011. Controls on preferential recharge to Chalk aquifers. *Journal of Hydrology,* **398**(1), pp. 109-123.

JAFARI, G.R., PEDRAM, P. and HEDAYATIFAR, L., 2012. *Erratum: long-range correlation and multifractality in bachs inventions pitches.*

KANTELHARDT, J.W., KOSCIELNY-BUNDE, E., REGO, H., HAVLIN, S. and BUNDE, A., 2001. Detecting long-range correlations with detrended fluctuation analysis. *PHYSICA A,* **295**(3-4), pp. 441-454.

KAVASSERI, R.G. and NAGARAJAN, R., 2004. Evidence of crossover phenomena in wind speed data. *IEEE Transactions on Circuits and Systems,* **51**(11), pp. 2255.

KOSCIELNY-BUNDE, E., BUNDE, A., HAVLIN, S. and GOLDREICH, Y., 1996. Analysis of daily temperature fluctuations. *Physica A: Statistical Mechanics and its Applications,* **231**(4), pp. 393-396.

KOSCIELNY-BUNDE, E., KANTELHARDT, J.W., BRAUN, P., BUNDE, A. and HAVLIN, S., 2006. Long- term persistence and multifractality of river runoff records: Detrended fluctuation studies. *Journal of Hydrology,* **322**(1), pp. 120-137.

LABAT, D., MASBOU, J., BEAULIEU, E. and MANGIN, A., 2011. Scaling behavior of the fluctuations in stream flow at the outlet of karstic watersheds, France. *Journal of Hydrology,* **410**(3), pp. 162-168.

LI, E., MU, X., ZHAO, G. and GAO, P., 2015. Multifractal Detrended Fluctuation Analysis of Streamflow in the Yellow River Basin, China. *Water,* **7**(4), pp. 1670-1686.

LI, Z. and ZHANG, Y., 2007. Quantifying fractal dynamics of groundwater systems with detrended fluctuation analysis. *Journal of Hydrology,* **336**(1), pp. 139-146.

LIANG, X. and ZHANG, Y., 2013. Temporal and spatial variation and scaling of groundwater levels in a bounded unconfined aquifer. *Journal of Hydrology,* **479**, pp. 139-145.

LITTLE, M.A. and BLOOMFIELD, J.P., 2010. Robust evidence for random fractal scaling of groundwater levels in unconfined aquifers. *Journal of Hydrology,* **393**(3), pp. 362-369.

MARSH, T. and HANNAFORD, J., 2008. *UK hydrometric register: Hydrological data UK.* Wallingford: Centre for Ecology and Hydrology.

MATSOUKAS, C., ISLAM, S. and RODRIGUEZ-ITURBE, I., 2000. Detrended fluctuation analysis of rainfall and streamflow time series. *Journal of Geophysical Research: Atmospheres,* **105**(D23), pp. 29165-29172.

NATIONAL CANCER INSTITUTE, 2016. *Joinpoint Trend Analysis Software.* National CancerInstitute.

OZGER, M., 2011. Scaling characteristics of ocean wave height time series. *Physica A: Statistical Mechanics and its Applications,* **390**(6), pp. 981-989.

PARRY, S., MARSH, T. and KENDON, M., 2013. 2012: from drought to floods in England and Wales. *Weather,* **68**(10), pp. 268-274.

PENG, C.K., BULDYREV, S.V., HAVLIN, S., SIMONS, M., STANLEY, H.E. and GOLDBERGER, A.L., 1994. Mosaic organization of DNA nucleotides. *Physical review.E, Statistical physics, plasmas, fluids, and related interdisciplinary topics,* **49**(2), pp. 1685.

PENG, C.K., HAVLIN, S., STANLEY, H.E. and GOLDBERGER, A.L., 1995. Quantification of scaling exponents and crossover phenomena in nonstationary heartbeat time series. *Chaos (Woodbury, N.Y.),* **5**(1), pp. 82.

POST, V. and ASMUTH, J., 2013. Review: Hydraulic head measurements - new technologies, classic pitfalls. *Hydrogeology Journal; Official Journal of the International Association of Hydrogeologists,* **21**(4), pp. 737-750.

REBOREDO, J.C., RIVERA-CASTRO, M., MIRANDA, J.G.V. and GARCÍA-RUBIO, R., 2013. How fast do stock prices adjust to market efficiency? Evidence from a detrended fluctuation analysis. *Physica A: Statistical Mechanics and its Applications,* **392**(7), pp. 1631-1637.

RUSSIAN, A., DENTZ, M., BORGNE, T., CARRERA, J. and JIMENEZ-MARTINEZ, J., 2013. Temporal scaling of groundwater discharge in dual and multicontinuum catchment models. *Water Resources Research,* **49**(12), pp. 8552-8564.

SADEGH MOVAHED, M., JAFARI, G.R., GHASEMI, F., RAHVAR, S. and REZA, R.T., 2006. Multifractal detrended fluctuation analysis of sunspot time series. *Journal of Statistical Mechanics: Theory and Experiment,* (02), pp. P02003-P02003.

SHANG, P., LU, Y. and KAMAE, S., 2008. Detecting long-range correlations of traffic time series with multifractal detrended fluctuation analysis. *Chaos, Solitons and Fractals,* **36**(1), pp. 82-90.

SIMON, A. and COLLISON, A., 2002. Quantifying the mechanical and hydrologic effects of riparian vegetation on streambank stability. *Earth Surface Processes and Landforms,* **27**(5), pp. 527-546.

SORENSEN, J.P.R. and BUTCHER, A.S., 2011. Water level monitoring pressure transducers - A need for industry-wide standards. *Ground Water Monitoring & Remediation,* **31**(4), pp. 56-62.

TELESCA, L. and LOVALLO, M., 2012. Analysis of temporal fluctuations in Bach's sinfonias. *Physica A: Statistical Mechanics and its Applications,* **391**(11), pp. 3247-3256.

TESSIER, Y., LOVEJOY, S., HUBERT, P. and SCHERTZER, D., 1996. Multifractal analysis and modeling of rainfall and river flows and scaling, causal transfer functions. *Journal of Geophysical Research: Atmospheres,* **101**, pp. 26427-26440.

WEEKS, E.P., 2002. The Lisse Effect Revisited. *Ground Water,* **40**(6), pp. 652-656.

WILLIAMS, Z.C. and PELLETIER, J.D., 2015. Self-affinity and surface-area-dependent fluctuations of lake-level time series. *Water Resources Research,* **51**(9), pp. 7258-7269.

YU, X., GHASEMIZADEH, R., PADILLA, I.Y., KAELI, D. and ALSHAWABKEH, A., 2016. Patterns of temporal scaling of groundwater level fluctuation. *Journal of Hydrology,* **536**, pp. 485-495.

ZHANG, J., GONG, H., ROSS, M.A., XIAOJUAN, L. and DEMIN, Z., 2011. Numerical modeling of shallow water table behavior with Lisse effect. *Chinese Geographical Science,* **21**(2), pp. 249-256.

ZHANG, Q., ZHOU, Y., SINGH, V.P. and CHEN, Y.D., 2011. Comparison of detrending methods for fluctuation analysis in hydrology. *Journal of Hydrology,* **400**(1–2), pp. 121-132.

ZHANG, Y. and SCHILLING, K., 2004. Temporal scaling of hydraulic head and river base flow and its implication for groundwater recharge. *Water Resources Research,* **40**(3), pp. W035041-W035049.

ZHANG, Y. and YANG, X., 2010. Effects of variations of river stage and hydraulic conductivity on temporal scaling of groundwater levels: Numerical simulations. *Stochastic Environmental Research and Risk Assessment,* **24**(7), pp. 1043-1052.

ZHU, J., YOUNG, M.H. and OSTERBERG, J., 2012. Impacts of riparian zone plant water use on temporal scaling of groundwater systems. *Hydrological Processes,* **26**(9), pp. 1352-1360.

ZUNINO, L., TABAK, B.M., FIGLIOLA, A., PÉREZ, D.G., GARAVAGLIA, M. and ROSSO, O.A., 2008. A multifractal approach for stock market inefficiency. *Physica A: Statistical Mechanics and its Applications,* **387**(26), pp. 6558-6566.

Appendix A – Procedure for the removal of the Lisse effect

In the absence of soil air pressure data and other identifiers that would indicate a Lisse event from one that is otherwise, the following systematic approach was implemented for the removal of the Lisse effect:

- Gradients in the time series that exceed a pre-defined positive and negative threshold are identified. In this way the start and end of a Lisse event are identified. The thresholds are selected based on the probability density function of the slopes and on trial and error.
- Data points identified as being within a Lisse event are clustered using K-means clustering in order to segregate individual Lisse events.
- The clustering was assessed visually, and if necessary, amended.
- A linear slope joining the start and end of each Lisse event was computed to replace the Lisse event.

Figure A. 1 illustrates some Lisse events observed in the GWL data from Wallingford and the computed linear slope that will replace them.

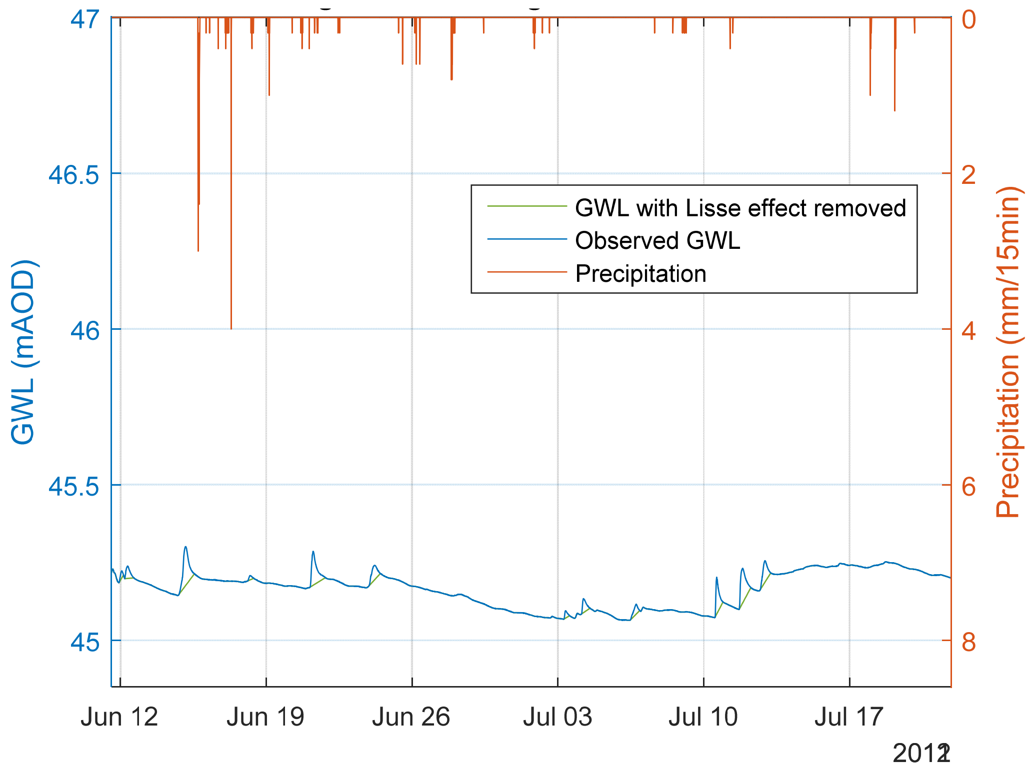

Figure A. 1 Illustration of the removal of some Lisse events from the Wallingford site